Organic transistors manufactured using inkjet technology with subfemtoliter accuracy

Tsuyoshi Sekitani*, Yoshiaki Noguchi*, Ute Zschieschang†, Hagen Klauk†, and Takao Someya*‡

*Quantum-Phase Electronics Center, School of Engineering, University of Tokyo, 7-3-1 Hongo, Bunkyo-ku, Tokyo 113-8656, Japan; and †Max Planck Institute for Solid State Research, Heisenbergstrasse 1, 70569 Stuttgart, Germany

Edited by Zhenan Bao, Stanford University, Stanford, CA, and accepted by the Editorial Board February 7, 2008 (received for review September 5, 2007)

A major obstacle to the development of organic transistors for large-area sensor, display, and circuit applications is the fundamental compromise between manufacturing efficiency, transistor performance, and power consumption. In the past, improving the manufacturing efficiency through the use of printing techniques has inevitably resulted in significantly lower performance and increased power consumption, while attempts to improve performance or reduce power have led to higher process temperatures and increased manufacturing cost. Here, we lift this fundamental limitation by demonstrating subfemtoliter inkjet printing to define metal contacts with single-micrometer resolution on the surface of high-mobility organic semiconductors to create high-performance p-channel and n-channel transistors and low-power complementary circuits. The transistors employ an ultrathin low-temperature gate dielectric based on a self-assembled monolayer that allows transistors and circuits on rigid and flexible substrates to operate with very low voltages.

inkjet printing | organic electronics | self-assembled monolayer

To realize a sustainable society, it is imperative that industrial manufacturing processes undergo a transformation with minimal impact on the environment. From this viewpoint, emerging printable electronics technology (1–6) has attracted considerable attention because it has the potential to drastically reduce ecological footprints and the energy consumed in manufacturing. Moreover, this technology is expected to reduce the material wastage that results from the use of a particular quantity of ink at a certain location.

In particular, digital fabrication that employs inkjet technology is expected to play an important role in industrial manufacturing processes because this technique can be applied for patterning high-purity electrically functional materials without preparing original patterning masks (7, 8). This application would consequently lead to a reduction in manufacturing costs and/or turnaround time. Inkjet technology has recently proliferated into the area of mass production of color filters for liquid crystal displays (9, 10); this further indicates that this would be the right time for the emergence of printed electronics.

However, there still exists a rather wide gap between the resolution required for high-performance electronic devices, such as transistors, and the typical resolution of conventional inkjet printers. For example, microprocessors based on single-crystal silicon field-effect transistors with a gate length of 32 nm are now in mass production (11), and active-matrix liquid-crystal displays in notebook computers and flat-screen television sets employ amorphous-silicon thin-film transistors (TFTs) with a channel length of $\approx$2 μm. On the other hand, an inkjet print head typically maintains a discharge volume on the order of several picoliters, which creates dots with a minimum diameter of $\approx$30–50 μm on regular paper. The minimum size of a droplet ejected from an inkjet head determines the printing resolution, and it is, in principle, limited by surface tension. This makes it difficult to reduce the droplet volume below $\approx$1 pl.

The present work demonstrates the feasibility of employing inkjet technology with subfemtoliter droplet volume and single-micrometer resolution for electronic device applications. We have manufactured p-channel and n-channel organic TFTs with source/drain contacts prepared by subfemtoliter inkjet printing of Ag nanoparticles deposited directly on the surface of the organic semiconductor layers, without the need for any photolithographic prepatterning (12, 13) or any surface pretreatment (14, 15). This allows us to prepare top-contact TFTs with a channel length of 1 μm. In contrast to bottom-contact TFTs (in which the contacts are defined before the deposition of the organic semiconductor and hence the channel length can be very small through the use of photolithography or electron-beam lithography), top-contact TFTs benefit from significantly lower contact resistance (16) but require a contact patterning technique that does not harm the organic semiconductor (17). Because the amount of organic solvent dispensed during subfemtoliter inkjet printing is extremely small and the Ag nanoparticle calcination temperature after subfemtoliter inkjet printing is low (130°C), the morphology of the organic semiconductors is not disturbed. As a result, TFTs that combine short channel length (1 μm) with small contact resistance (5 kΩ·cm) and small parasitic capacitance are demonstrated.

Results

The TFTs employ vacuum-evaporated aluminum gate electrodes patterned by shadow-masking and a gate dielectric based on a combination of a thin layer of aluminum oxide (3.6 nm thick) and a molecular self-assembled monolayer (SAM) of *n*-octadecylphosphonic acid (2.1 nm thick) (18). The aluminum oxide film results from a brief oxygen-plasma treatment required to create a sufficient density of hydroxyl groups for molecular adsorption, and the SAM is prepared from a 2-propanol solution at room temperature. The gate dielectric capacitance is 0.7 μF/cm^2, so the TFTs operate with voltages between 2 and 3. Thirty-nanometer-thick films of pentacene and hexadecafluorocopperphthalocyanine (F_{16}CuPc) are deposited in vacuum and patterned by shadow-masking to provide the semiconductor films for the p-channel (19, 20) and n-channel (21) TFTs, respectively.

A subfemtoliter inkjet printer (22, 23) is used to deposit narrow metal lines with single-micrometer accuracy directly on top of the pentacene and F_{16}CuPc layers. The subfemtoliter inkjet system is described in detail in *Materials and Methods*.

Author contributions: T. Sekitani, U.Z., H.K., and T. Someya designed research; T. Sekitani, Y.N., and U.Z. performed research; T. Sekitani, H.K., and T. Someya analyzed data; and T. Sekitani, H.K., and T. Someya wrote the paper.

The authors declare no conflict of interest.

This article is a PNAS Direct Submission. Z.B. is a guest editor invited by the Editorial Board.

Freely available online through the PNAS open access option.

‡To whom correspondence should be addressed. E-mail: someya@ap.t.u-tokyo.ac.jp.

This article contains supporting information online at www.pnas.org/cgi/content/full/0708340105/DCSupplemental.

Some features of our subfemtoliter inkjet system are similar to the electrohydrodynamic jet system recently reported by Park *et al.* (24), but an important difference is that our system is used to print metal nanoparticle inks directly onto the surface of high-mobility organic semiconductor films. The ''ink'' consists of monodispersed Ag nanoparticles with a diameter of 2~3 nm functionalized with a proprietary dispersing agent and suspended in tetradecane as a nonpolarized organic solvent (Harima Chemicals; NPS-J-HP, viscosity 10 mPa·s). The Ag content by volume is 10%. Calcination of the inkjet-printed lines at a temperature of 130°C for 1 h in nitrogen removes the dispersing agent and fuses the nanoparticles into a homogeneous metallic line with large electrical conductivity (22, 23, 25, 26). As a result, top-contact TFTs with high-resolution inkjet-printed source/drain contacts are obtained.

The performance of the subfemtoliter inkjet system is illustrated in Fig. 1. The Ag nanoparticle droplets dispensed from the inkjet nozzle have a volume of 0.7 ± 0.2 fl and a diameter of <1 μm in air. The diameter of the Ag dots thus created on the pentacene surface can be controlled between 2 μm and 6 μm, and the thickness of the dots is 30 nm. Fig. 1 *a* and *b* shows optical microscope and atomic force microscope (AFM) images of a pentacene film with an array of printed Ag dots after calcination with an average diameter of 2 ± 0.5 μm. The distinct morphology of the pentacene film and the excellent uniformity of the inkjet-printed metal dots are clearly seen. Fig. 1 *c* and *d* confirms that inkjet-printed metal lines with linewidths as small as 2 μm are uniform and continuous. Fig. 1*c* also shows that lines with a width of 1 μm can be created as well, although the uniformity is insufficient to guarantee metallic connectivity over long distances. Lines having a width of 2 μm, however, can be written uniformly and reproducibly over large areas, as shown in Fig. 1*d*.

To control the thickness and electrical conductance of the metal lines, multiple inkjet passes are performed. Fig. 1 *e* and *f* illustrates the evolution of the morphology and electrical resistivity of an inkjet-printed Ag line with an increasing number of passes. The effective thickness of the line increases linearly with the number of passes, from 30 nm after a single pass to 600 nm after 20 passes. After calcination (performed at a temperature of 130°C for 1 h in nitrogen), the line resistivity is measured at room temperature in air. Fig. 1*f* shows that 10 passes are sufficient to obtain continuous lines with a resistivity of <25 $\mu\Omega$·cm, which is sufficiently low for practical applications.

Compared with picoliter inkjet printing, subfemtoliter printing significantly reduces the calcination temperature required to achieve near-bulk metal resistivity. Low calcination temperatures are important for the manufacturing of top-contact devices because temperatures above ≈150°C will irreversibly damage the organic semiconductors (27, 28). Using the same Ag nanoparticle ink, but employing a conventional picoliter inkjet system, we obtained a resistivity of (56 ± 8) $\mu\Omega$·cm after calcination at 130°C, and a temperature well above 150°C was required to obtain a resistivity below 25 $\mu\Omega$·cm. With subfemtoliter printing, a calcination temperature of 130°C is sufficient to obtain a resistivity of 25 $\mu\Omega$·cm.

A schematic cross-section of the completed transistors is shown in Fig. 2*a*. We have manufactured TFTs with channel length ranging from 1 μm to 100 μm. Fig. 2*b* shows optical microscope images of pentacene TFTs with channel length of 1 μm, 2 μm, and 5 μm after calcination; in each case, the width of the inkjet-printed contact lines is 5 μm. Fig. 2*c* shows an AFM image of a TFT with a channel length of 5 μm.

The DC electrical characteristics of the TFTs were measured in air using a semiconductor parameter analyzer (Agilent 4156C). Fig. 3 *a* and *b* shows the current–voltage characteristics of a p-channel pentacene TFT with a channel length of

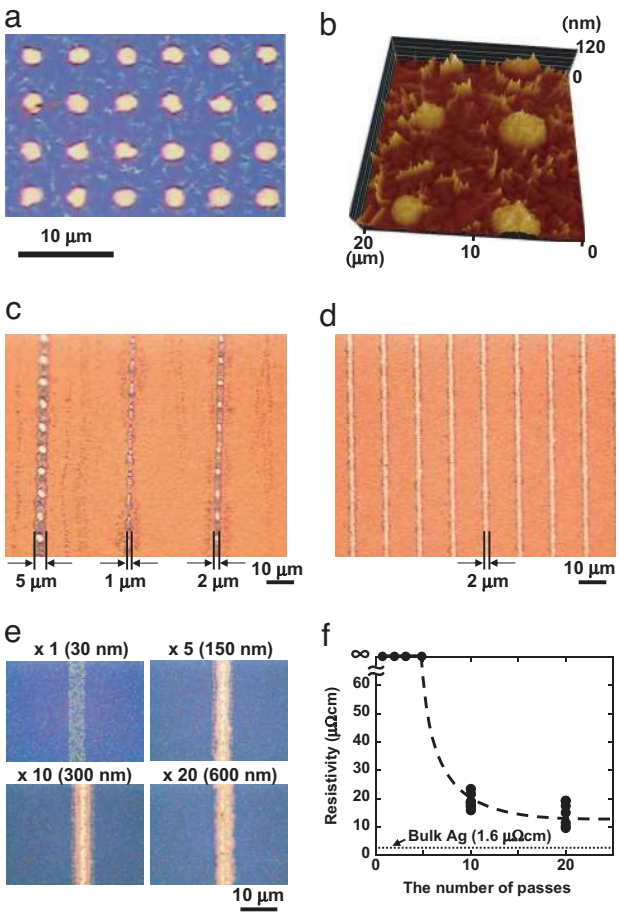

Fig. 1. Printed Ag nanoparticles using subfemtoliter inkjet. (*a* and *b*) Optical microscope image (*a*) and atomic force microscope (AFM) image (*b*) of fine dots of Ag nanoparticles deposited by subfemtoliter inkjet printing on the surface of a thin pentacene film after calcination at 130°C. The diameter of the dots is ≈2 μm, and the thickness is 30 nm. The dots were formed with a single printing pass. (*c*) Optical microscope image of inkjet-printed Ag lines after a single printing pass before calcination. Linewidths between 1 μm and 5 μm were obtained in a controlled manner by adjusting the electric field inside the inkjet nozzle. (*d*) Optical microscope image of inkjet-printed Ag lines after a single printing pass and after calcination at 130°C. Lines with a linewidth down to 2 μm are uniform and continuous over large areas. (*e*) Optical microscope image showing the effect of multiple-pass printing on the evolution of the morphology of an inkjet-printed Ag line after calcination. The effective thickness of the line increases from 30 nm after a single pass to 600 nm after 20 passes. (*f*) Evolution of the electrical resistivity of inkjet-printed Ag lines with the number of passes after calcination at 130°C for 1 h in nitrogen.

1 μm and a channel width of 300 μm. Because of the large capacitance of the thin gate dielectric (0.7 μF/cm^2), the TFTs show excellent linear and saturation characteristics for gate-source and drain-source voltages of 3 V. Despite the short channel length of 1 μm, the off-state current at V_{GS} = 0 V is <20 pA, and the on/off current ratio is ≈10^6. Despite the small thickness of the room-temperature gate dielectric, the maximum gate current at V_{GS} = −3 V is only ≈100 pA. Fig. 3 *c* and *d* summarizes results obtained from pentacene TFTs with channel lengths ranging from 1 μm to 100 μm, all having a channel width of 300 μm. The TFT resistance in the saturation regime scales linearly with channel length over the entire range of channel lengths, as predicted by field-effect transistor theory. By extrapolating the linear fit to a channel length of zero, an effective contact resistance of 5 kΩ·cm is extracted. This is smaller than the contact resistance of pentacene TFTs

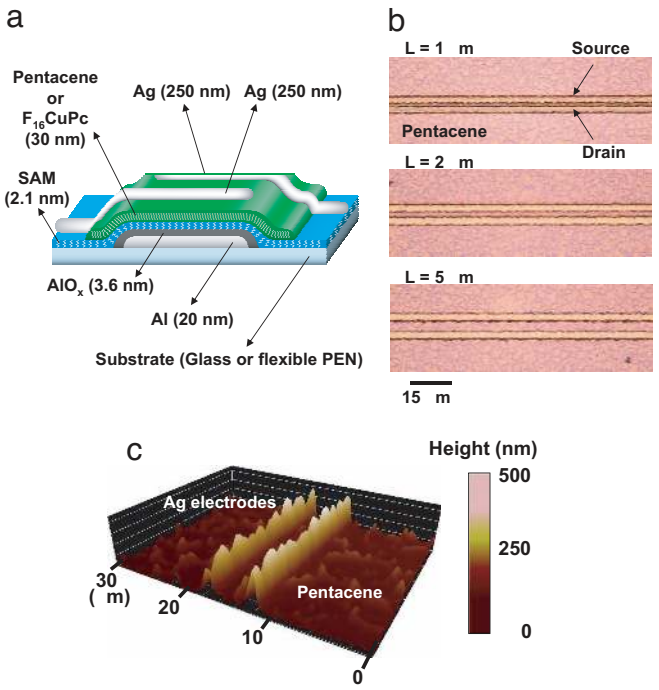

Fig. 2. Structure, micrograph, and AFM image of organic transistors. (*a*) Schematic cross-section of the organic thin-film transistors with patterned Al gates, ultrathin gate dielectric, vacuum-deposited organic semiconductor, and subfemtoliter inkjet-printed Ag nanoparticle source/drain contacts. (*b*) Optical microscope images of pentacene TFTs with channel length of 1 μm, 2 μm, and 5 μm after calcination (the linewidth of the inkjet-printed contact lines is 5 μm). (*c*) AFM image of a pentacene TFT with a channel length of 5 μm and a contact linewidth of 2 μm.

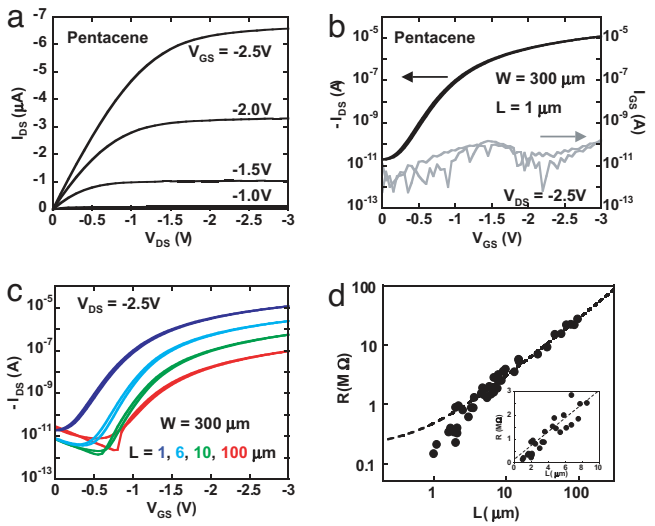

Fig. 3. Transistor characteristics of p-type pentacene TFTs. (*a* and *b*) Output (*a*) and transfer (*b*) characteristics of a p-channel pentacene TFT with a channel length of 1 μm and a channel width of 300 μm. The measurements were carried out in air. (*c*) Transfer characteristics of pentacene TFTs with channel length of 1 μm, 6 μm, 10 μm, and 100 μm, showing the scaling of the maximum drain current with channel length (channel width is 300 μm for all devices). The measurements were taken on TFTs prepared without substrate heating during the pentacene deposition. (*d*) The resistance of pentacene TFTs in the saturation regime scales linearly with channel length, as predicted by field-effect transistor theory. By extrapolating the linear fit to a channel length of zero, a contact resistance of 5 kΩ·cm is extracted.

with bottom contacts (16) and identical to the contact resistance of pentacene TFTs with evaporated Ag top contacts (29), which confirms the high quality of the interface between the organic semiconductor and the inkjet-printed contacts. Depending on the pentacene deposition conditions, the field-effect mobility of the TFTs is between 0.03 cm^2/Vs (substrates not heated during pentacene deposition) and 0.3 cm^2/Vs (pentacene deposited onto substrates held at a temperature of 60°C during the vacuum deposition). These mobilities are comparable to those obtained with evaporated Au source/drain contacts, suggesting that the mobility is not affected by the 130°C calcination. This is consistent with our previous work (27, 28) and with our observation that the morphology of the pentacene films (examined by AFM) does not change during calcination at 130°C. Other authors have reported changes in pentacene morphology and mobility degradation during annealing (30, 31). The reason for this discrepancy is unknown but possibly related to the different gate dielectric materials—i.e., organic dielectrics (polyimide or self-assembled monolayer) versus inorganic dielectrics (SiO_2).

An additional benefit of the subfemtoliter inkjet device process described here is that small gate-to-source and gate-to-drain overlap areas are easily obtained even without precise alignment of the contacts with respect to the gate electrode, and without the use of self-alignment schemes (14, 15, 32–34). For example, the pentacene TFT shown in Fig. 3 *a* and *b* has a parasitic capacitance of only 6 pF. With a carrier mobility of 0.3 cm^2/Vs, this translates into a cutoff frequency above 2 MHz—about five orders of magnitude faster than the best result reported to date for printed organic circuits (35).

The output and transfer characteristics of an n-channel F_{16}CuPc TFT are shown in Fig. 4 *a* and *b*. It has a carrier mobility of 0.02 cm^2/Vs and an on/off current ratio of $>10^4$. These parameters are essentially identical to those of F_{16}CuPc TFTs with evaporated metal contacts (18), which again confirms the excellent performance of the printed contacts. The minimum feature size we have obtained when printing on F_{16}CuPc is essentially identical to the feature size obtained by printing on pentacene—i.e., dot diameter and linewidth can be controlled between 2 μm and 7 μm, and the thickness is 30 nm [see supporting information (SI) Fig. S1].

Using p-channel pentacene TFTs and n-channel F_{16}CuPc TFTs with patterned Al gates, SAM-based gate dielectric, and inkjet-printed source/drain contacts, we have also prepared organic complementary inverters. A photograph and the electrical transfer characteristics of such an inverter are shown in Fig. 4 *c* and *d*. The pentacene TFT has a channel length of 50 μm, the F_{16}CuPc TFTs has a channel length of 5 μm, and both TFTs have a channel width of 60 μm. The difference in channel length is necessary to achieve similar drain currents for both TFTs despite the significant difference in carrier mobility (0.1 cm^2/Vs for the pentacene TFT, 0.02 cm^2/Vs for the F_{16}CuPc TFT). The inverter operates with supply voltages between 1.5 V and 3 V and with a small-signal gain >10. From a circuit design perspective, complementary circuits have several advantages over circuits based on a single carrier type, including greater noise margin, lower power consumption, and faster switching speed (36).

Discussion

With the manufacturing process described here, all three geometry parameters that contribute to the high-frequency performance of organic TFTs are scaled simultaneously and with an aggressiveness unprecedented in printed electronics. First of all, the channel length of the TFTs is reduced to 1 μm, which is the shortest channel length reported for organic TFTs with patterned gates and printed source/drain contacts. Im-

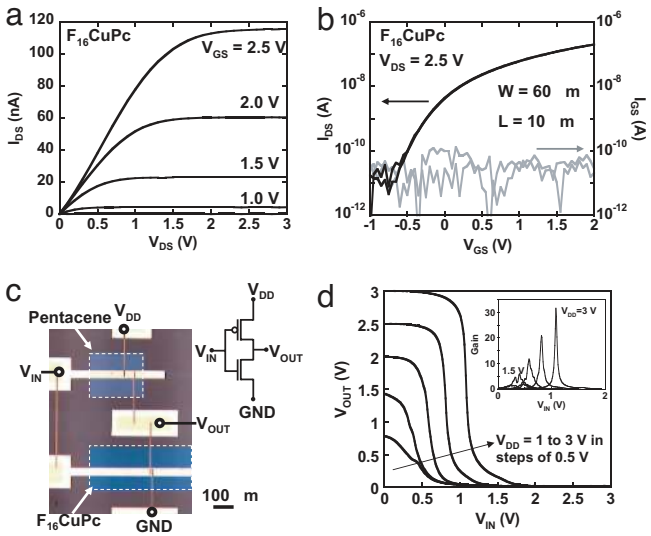

Fig. 4. Electrical characteristics of n-type $F_{16}CuPc$ TFTs and organic CMOS inverter. (*a* and *b*) Output (*a*) and transfer (*b*) characteristics of an n-channel $F_{16}CuPc$ TFT with a channel length of 10 μm and a channel width of 60 μm. The measurements were carried out in air. (*c* and *d*) Optical microscope image (*c*) and transfer characteristics (*d*) of an organic complementary inverter. The pentacene TFT has a channel length of 50 μm, the $F_{16}CuPc$ TFT has a channel length of 5 μm, and both TFTs have a channel width of 60 μm. The inverter operates with supply voltages between 1.5 V and 3 V and with a small-signal gain >10.

portantly, this short channel length is obtained along with low contact resistance because a top-contact structure is used. Second, the gate dielectric thickness is reduced to a few nanometers without introducing prohibitive gate leakage. This means that the TFTs can be operated with low voltages (3 V) while also assuring that the TFTs have very small off-state currents ($\approx$20 pA), a large on/off current ratio ($\approx 10^6$), and excellent drain current saturation even at small drain-source voltages. Finally, the parasitic capacitance of the transistors is reduced to a few picofarads because the printed source/drain contacts have a linewidth of only 2 μm. This extraordinary miniaturization of the key transistor parameters is achieved within the boundaries of a low-temperature, flexible-substrate-compatible, low-cost, large-area manufacturing approach.

The fact that the source/drain contacts can be inkjet-printed on top of the pentacene and $F_{16}CuPc$ surfaces without destroying the organic semiconductors is a direct consequence of the small volume of the droplets ejected from the subfemtoliter inkjet head. Because the droplet volume is so small (diameter <1 μm in air), the organic solvent evaporates before the droplet reaches the semiconductor surface, so that the organic semiconductor films are not harmed by the solvents and there is no significant spreading of the nanoparticle droplets on the surface (diameter $\approx$2 μm on the surface). Furthermore, the small size and large surface area of the droplets on the surface (thickness $\approx$30 nm) reduces the temperature required to remove the dispersing agent and fuse the nanoparticles into a metallic line with large electrical conductivity (25 $\mu\Omega$·cm at 130°C). Printing the same ink with a picoliter inkjet system, we have obtained droplets on the surface with a diameter of 50 μm and a thickness of 150 nm, which require a calcination temperature of 150°C, along with significant changes in the morphology of the organic semiconductor film.

Although other nonlithographic patterning techniques have been used to manufacture organic TFTs with micrometer and submicrometer dimensions (12–15, 37), these methods usually require prepatterning processes based on original patterning forms such as photolithography masks, or they work only with low-mobility semiconductors. In our study, ultrafine patterning with single-micrometer resolution is demonstrated on high-mobility p-channel and n-channel organic semiconductors simply by digital fabrication without any prepatterning processes or original patterning forms. The main limitation of the subfemtoliter inkjet system described here is the relatively small throughput, which is a consequence of the time required to cover large areas with multiple printing passes. Therefore, we believe that future manufacturing schemes for large-area printed electronic systems will benefit from the use of high-resolution subfemtoliter inkjet printing solely for the definition of critical device features, such as source/drain contacts for short-channel TFTs, while employing high-throughput, low-resolution printing techniques, such as picoliter inkjet printing, screen printing and gravure printing, to define large-area features that require lower accuracy, such as bitlines, wordlines, and interconnects.

Materials and Methods: Subfemtoliter Inkjet System

The nozzle of the subfemtoliter inkjet system is manufactured from a very fine capillary glass tube with a tip diameter of <1 μm. The inside of the capillary tube is hydrophilic, whereas the outside of the tube is hydrophobic. A pressure controller is used to control the pressure inside the tube. A fine electrically conducting wire is located inside the nozzle to charge the ink, and electric pulses with a voltage of <200 V are applied to eject droplets with subfemtoliter volume. The ejected droplets travel straight through the electric flux line. The accuracy of the mechanical *xy*-stage is better than 1 μm. The substrate is at room temperature.

ACKNOWLEDGMENTS. We thank Dr. Y. Matsuba (Harima Chemicals) for providing high-quality Ag nanoparticles, Dr. K. Murata and K. Shimizu (SIJ Technology) for technical support in the inkjet process, and Benjamin Stuhlhofer (Max Planck Institute for Solid State Research) for expert technical assistance. This work was partially supported by Special Coordination Funds for Promoting Science and Technology; the Ministry of Education, Culture, Sports, Science, and Technology; and the New Energy and Industrial Technology Development Organization.

1. Service RF (2004) *Science* 304:675.
2. Katz HE (2004) *Chem Mater* 16:4748–4756.
3. Rogers JA (2001) *Science* 291:1502–1503.
4. Hamedi M, Forchheimer R, Inganäs O (2007) *Nat Mater* 6:357–362.
5. Garnier F, Hajlaoui R, Yassar A, Srivastava P (1994) *Science* 265:1684–1686.
6. Rogers JA, Bao ZN, Baldwin K, Dodabalapur A, Crone B, Raju VR, Kuck V, Katz H, Amundson K, Ewing J, Drzaic P (2001) *Proc Natl Acad Sci USA* 98:4835–4840.
7. Calvert P (2001) *Chem Mater* 13:3299–3305.
8. de Gans BJ, Duineveld PC, Schubert US (2004) *Adv Mater* 16:203–213.
9. Bharathan J, Yang Y (1998) *Appl Phys Lett* 72:2660–2662.
10. Sirringhaus H, Wilson RJ, Friend RH, Inbasekaran M, Wu W, Woo EP, Grell M, Bradley DDC (2000) *Appl Phys Lett* 77:406–408.
11. Bai P, Auth C, Balakrishman S, Bost M, Brain R, Chikarmane V, Heussner R, Hussein M, Hwang J, Ingerly D, *et al.* (2004) *Tech Dig Int Electron Devices Meet*, pp 657–660.
12. Sirringhaus H, Kawase T, Friend RH, Shimoda T, Inbasekaran M, Wu W, Woo EP (2000) *Science* 290:2123–2126.
13. Wang JZ, Zheng ZH, Li HW, Huck WTS, Sirringhaus H (2004) *Nat Mater* 3:171–176.
14. Stutzmann N, Friend RH, Sirringhaus H (2003) *Science* 299:1881–1884.
15. Sele CW, Werne T, Friend RH, Sirringhaus H (2005) *Adv Mater* 17:997–1001.
16. Necliudov PV, Shur MS, Gundlach DJ, Jackson TN (2003) *Solid-State Electron* 47:259–262.
17. Gundlach DJ, Jackson TN, Schlom DG, Nelson SF (1999) *Appl Phys Lett* 74:3302–3304.
18. Klauk H, Zschieschang U, Pflaum J, Halik M (2007) *Nature* 445:745–748.
19. Dimitrakopoulos CD, Malenfant PRL (2002) *Adv Mater* 14:99–117.
20. Klauk H, Gundlach DJ, Nichols JA, Jackson TN (1999) *IEEE Trans Electron Devices* 46:1258–1263.
21. Bao Z, Lovinger A, Brown J (1998) *J Am Chem Soc* 120:207–208.
22. Murata K, Matsumoto J, Tezuka A, Matsuba Y, Yokoyama H (2005) *Microsyst Technol* 12:2–7.
23. Murata K (2003) *Proceedings of the 2003 International Conference on MEMS, NANO, Smart Systems*, eds Badaway W, Moussa W (IEEE Computer Society, Washington, DC), pp 346–349.
24. Park JU, Hardy M, Kang SJ, Barton K, Adair K, Mukhopadhyay DK, Lee CY, Strano MS, Alleyne AG, Georgiadis JG, *et al.* (2007) *Nat Mater* 6:782–789.

25. Saito H, Matsuba Y (2006) *Proceedings of the 39th International Symposium on Microelectronics*, eds 2006 Technical Program Committee and the IMAPS Staff (International Microelectronics and Packaging Society, Washington, DC), pp 470–477.
26. Saito H, Ueda M, Oyama K, Matsuba Y (2005) *Proceedings of the International Conference on Electronics Packaging*, eds 2005 Technical Program Committee of ICEP (International Microelectronics and Packaging Society, Washington, DC), pp 259–262.
27. Sekitani T, Iba S, Kato Y, Someya T (2004) *Appl Phys Lett* 85:3902–3904.
28. Sekitani T, Someya T, Sakurai T (2006) *J Appl Phys* 100:024513.
29. Pesavento PV, Chesterfield RJ, Newman CR, Frisbie CD (2004) *J Appl Phys* 96:7312–7324.
30. Kang SJ, Noh M, Park DS, Kim HJ, Whang CN, Chang C-H (2004) *J Appl Phys* 95:2293–2296.
31. Ye R, Baba M, Suzuki K, Ohishi Y, Mori K (2003) *Jpn J Appl Phys* 42:4473–4475.
32. Ando M, Kawasaki M, Imazeki S, Sasaki H, Kamata T (2004) *Appl Phys Lett* 85:1849.
33. Lu JP, Mei P, Rahn J, Ho J, Wang Y, Boyce JB, Street RA (2000) *J Non-Cryst Solids* 266:1294–1298.
34. Nagai T, Naka S, Okada H, Onnagawa H (2007) *Jpn J Appl Phys* 46:2666–2668.
35. Hübler AC, Doetz F, Kempa H, Katz HE, Bartzsch M, Brandt N, Hennig I, Fuegmann U, Vaidyanathan S, Granstrom J, *et al.* (2007) *Org Electron* 8:480–486.
36. Crone BK, Dodabalapur A, Sarpeshkar R, Filas RW, Lin Y-Y, Bao Z, O'Neill JH, Li W, Katz HE (2001) *J Appl Phys* 89:5125–5132.
37. Noh YY, Zhao N, Caironi M, Sirringhaus H (2007) *Nat Nanotechnol* 2:784–789.

Supporting Information

Sekitani *et al.* 10.1073/pnas.0708340105

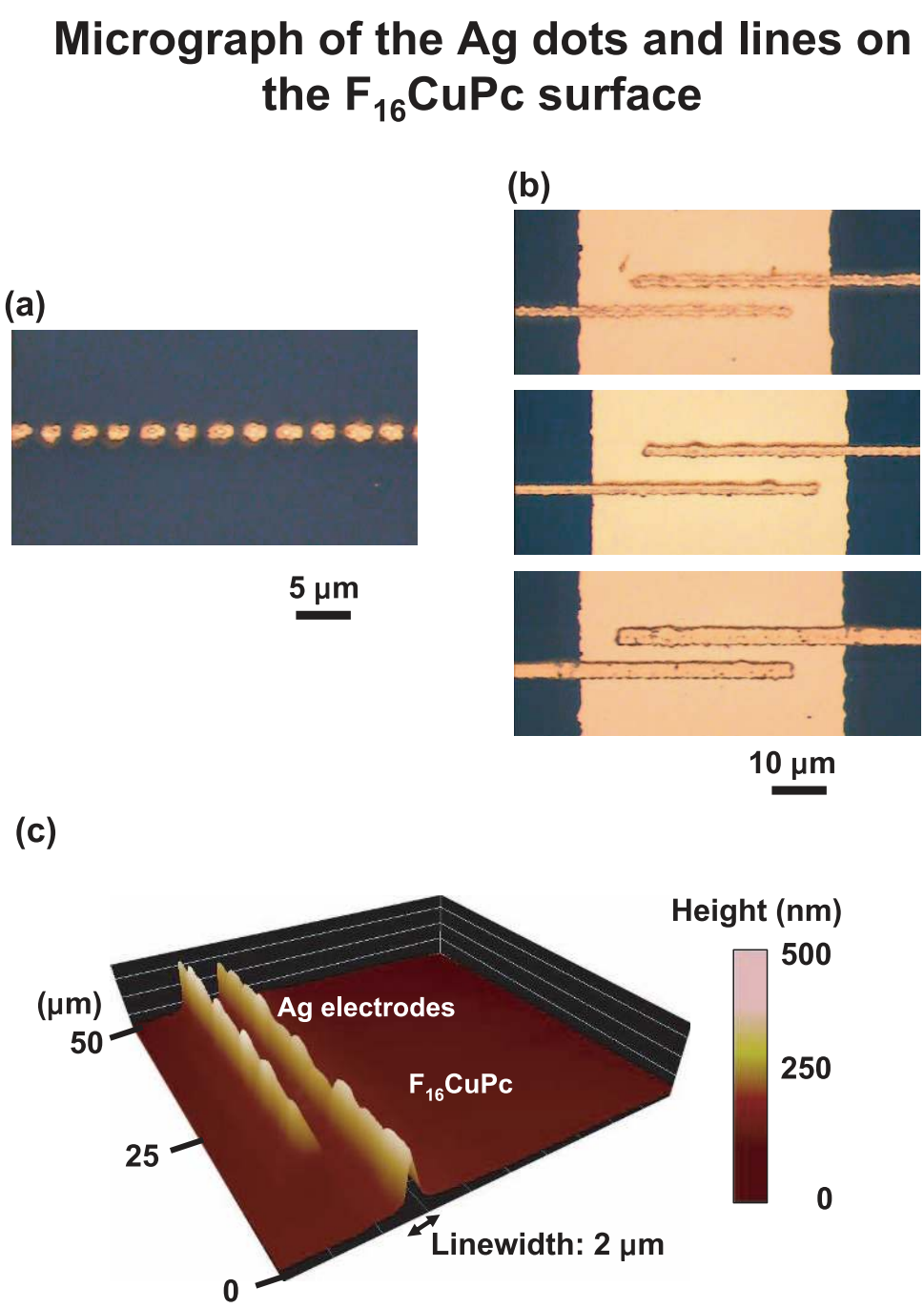

Fig. S1. Optical microscope and atomic force microscope (AFM) images of inkjet-printed Ag lines on the surface of the *n*-channel organic semiconductor F_{16}CuPc. (*a*) Ag dots created on the F_{16}CuPc surface. The diameter of the dots is ≈2 μm, and the thickness of the dots is 30 nm. (*b*) Ag lines created on the F_{16}CuPc surface, which can be controlled between 2 and 7 μm linewidth. These dimensions are essentially the same as those on the pentacene surface. (*c*) AFM image of the lines on the F_{16}CuPc. The linewidth is 2 μm.